

MITIGATION OF NUMERICAL NOISE FOR SPACE CHARGE CALCULATIONS IN TRACKING CODES

L.G. Vorobiev, C. Ankenbrandt, T.J. Roberts, Muons, Inc., Batavia, IL 60510, USA
F. Schmidt, CERN, Geneva, Switzerland

Abstract

Modern tracking codes have very stringent requirements concerning space charge calculations. They should combine speed of calculations, in order to track particles for many turns (e.g. the LHC injection chain), with numerical accuracy while maintaining symplecticity. Grid solvers and modified Green's function algorithms have been compared, and upgrades were suggested.

INTRODUCTION

Multiple-particle tracking allows for accurate space charge (SC) beam simulations and design. However, in the particle-in-cell (PIC) formalism [1], spatial non-physical grid effects may jeopardize the validity of modeling in accelerator rings and colliders, especially during multi-turn particle tracking. To remedy artificial grid noise, PIC codes increasingly use more macro-particles, denser grids, and more SC kicks per bunch, requiring massive parallelization. Even so, numerical errors persist. The split operator method itself (unlike the general PIC paradigm) decouples three-dimensional (3D) SC forces and dynamics, possibly resulting in additional errors and faulty estimates of instabilities, dynamic aperture, emittance growth, etc. Recent numerical experiments demonstrated artificial noise due to mesh effects and interpolation, leading to micro-scale beam instability [2].

The situation can be improved in two ways. First, we perfect the components of the PIC formalism itself. We will develop a grid density module, suppressing numerical noise to upgrade the accuracy of Poisson solvers. Secondly, we avoid spatial grids entirely, because despite precautions the grid-related noise will always persist. The known grid-free SC solvers are based on the classic Green's function or direct Vlasov solvers (we are aware only of axi-symmetric ones) [3], but they are too slow for multiple particle tracking in rings and work only in free space without boundaries. Instead, we introduce hybrid SC solvers based on "space-charge templates", which represent macro Green's functions for macro-elements [4-5], from which a large family of beam distributions can be built. These SC templates calculate the 3D self-forces of a beam in the presence of conducting boundaries.

There is a gap in terms of generality and performance between fast but over-simplified "frozen" models and standard PIC codes. The proposed hybrid SC solvers fill that gap: they are more flexible than "frozen" models and approach the accuracy of PICs while being much faster. Template-based solvers can simulate rather arbitrary beam distributions within conducting boundaries and may be parallelized, boosting their performance even further.

ACCURACY OF MULTIPLE-PARTICLE TRACKING BY PICS

The computational flows of multiple-particle tracking codes are similar, and our analyses of the accuracy and performance of their components have much in common.

PIC Computational Modules

Each macro-particle in a 3D beam has six phase space coordinates, and a step-by-step evolution of the ensemble of N macro-particles $\mathbf{X}=(x_1, x'_1, y_1, y'_1, z_1, z'_1, \dots, x_N, x'_N, y_N, y'_N, z_N, z'_N)$ looks like the following:

$$\mathbf{X}_{\text{old}} \rightarrow \underbrace{\rho_{3D}, u_{3D}, \mathbf{E}_{3D}}_{\text{Space Charge module}} \rightarrow \left[\begin{array}{c} \text{Trajectory} \\ \text{Integrator} \end{array} \right] \rightarrow \mathbf{X}_{\text{new}} \quad (1).$$

Here the trajectories are integrated either by multi-step (2nd order leap-frog, or higher order) schemes, or symplectic maps, which are more customary for multi-turn modeling in the rings. These higher order maps take into account non-linearities of the lattice and SC forces, and they trace particles with any prescribed accuracy in the framework of the single particle approximation [6].

Contemporary Poisson solvers are able to derive nearly exact grid solutions by multi-grid techniques, assuming that the input, i.e. the grid density, is known exactly. The interpolation between grid nodes is also very accurate. Unfortunately, the grid density is evaluated only approximately, and moreover, it represents the main source of numerical noise in (1). We need to find remedies to manage this.

Space Charge Density on the Grid

The Cloud-In-Cell (CIC) technique was developed decades ago (see [1] and references therein). If a spatial grid has dimensions of $N_x \times N_y \times N_z$ and meshes $h_x \times h_y \times h_z$, then the macro-particle sizes are $\delta_{x,y,z} = \Delta \times h_{x,y,z}$ ($\Delta \geq 0.5$). A redistribution of elementary space charge among grid nodes must satisfy a conservation of space charge and should converge for higher order interpolations. A linear scheme is used in ORBIT, WARP, and Synergia codes. A quadratic interpolation is also possible.

Using finite clouds with bell-like shape functions is beyond linear/quadratic interpolation. One needs an infinite polynomial series to represent them. For example, Fig. 1 shows a family of one dimensional (1D) clouds:

$$S_2(\xi) = \frac{q}{2\Delta}, S_3(\xi) = \frac{3q}{4\Delta} \left[1 - \frac{\xi^2}{\Delta^2} \right], S_4(\xi) = \frac{q}{2\Delta} \left[1 + \cos\left(\frac{\pi\xi}{\Delta}\right) \right],$$

$$S_5(\xi) = \frac{q}{3\Delta} \left[1 + \cos\left(\frac{\pi\xi}{\Delta}\right) \right]^2, S_6(\xi) = \frac{15q}{16\Delta} \left[1 - \frac{\xi^2}{\Delta^2} \right]^2 \text{ for } |\xi| \leq \Delta.$$

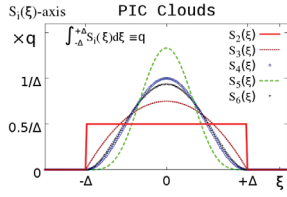


Figure 1: Macroparticle clouds in CIC scheme. All clouds have different ramps, but carry the same space charge "q".

As shown in [7], the integrals $\Phi_k = \int_a^{\eta} S_k(\xi) d\xi$ are:

$$\Phi_2(\eta, a) = q \frac{\eta - a}{2\Delta}, \quad \Phi_3(\eta, a) = q \frac{3(\eta - a)}{4\Delta} - q \frac{\eta^3 - a^3}{4\Delta^3},$$

$$\Phi_4(\eta, a) = q \frac{(\eta - a)}{2\Delta} - q \left(\sin \frac{\pi\eta}{\Delta} - \sin \frac{\pi a}{\Delta} \right) / 2\pi,$$

and so on for $\Phi_{5,6}(\eta, a)$. In our algorithm, the choice of the cloud may vary from the beam center to the edges. Figs. 2 illustrate SC density of 10^5 macro-particles within $40\text{cm} \times 40\text{cm}$ boundary, $N_x = N_y = 128$ and different sizes of macro-particles for the cloud $S_3(\xi)$.

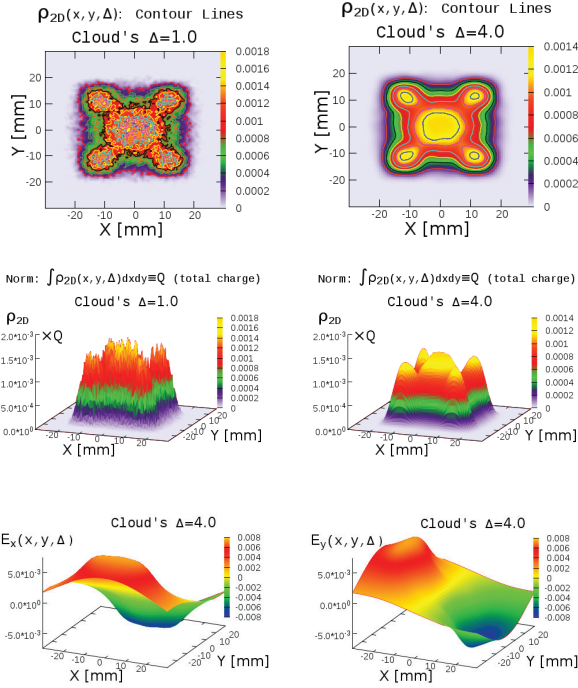


Figure 2: Contour plot (top), 3D space charge densities (middle) for $\Delta=1, 4$; and corresponding fields $E_{x,y}$ (bottom) for $\Delta=4$.

For $\Delta=1$ and 4 , contour lines and 3D plots are very different ($\sim 15\%$). The potentials, as integrals of densities differ by $< 0.01\%$. The field differences drop from 3% to less than 0.01% for $\Delta=1$ and 4 respectively [8].

SPACE CHARGE TEMPLATES

A concept of space charge templates was introduced in [5,9]. The templates are macro-elements reproducing an original beam; their fields are derived from the library of template fields via superposition. A family of beam

distributions built by templates is rather general but always has elliptical cross-sections along "z". See Fig. 3.

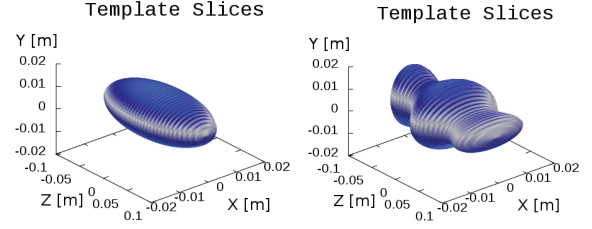


Figure 3: 3D beam bunches within a round cylindrical pipe of 4 cm in diameter (not shown). An ellipsoid $1\text{cm} \times 1\text{cm} \times 10\text{cm}$ (left) and an arbitrary 3D beam (right). Both bunches are "sliced" longitudinally by templates.

In earlier versions of space charge templates, the fields of a 3D beam were calculated, using a library of charged disks/slices with pre-assigned density distributions.

A more universal way to model a composite structure of real charge distributions is to use template-rings [10,8].

The 3D potential in free space \mathcal{R} is

$$u_{tmp}(\mathbf{x}) = \iiint_{\mathcal{R}} \rho(\tilde{\mathbf{x}}) d\tilde{\mathbf{x}} / |\mathbf{x} - \tilde{\mathbf{x}}|.$$

For the particular case of a round ring of the outer radius R_{tmp} and the inner radius $R_{tmp} - dR$ (dR_{tmp} stands for the thickness) with constant surface density σ_{tmp} , the potential becomes:

$$u_{tmp}(\mathbf{x}) = 2\pi\sigma_{tmp} \left[\sqrt{R_{tmp}^2 + z^2} - \sqrt{(R_{tmp} - dR)^2 + z^2} \right] \quad (2),$$

leading to analytical formulae for the longitudinal field on the axis [10]. We used this equation along with successive over-relaxation (SOR 3D) technique, which solves the Poisson equation with and without boundaries.

For illustration, the potentials of a positively charged disk of $R=0.01$ m, a negatively charged disk of $R=0.007$ m, a ring, as a superposition of these disks and a ring field are plotted in Fig. 4 (left). Template fields, representing a beam from right part of Fig. 3 are plotted in Fig. 4 (right).

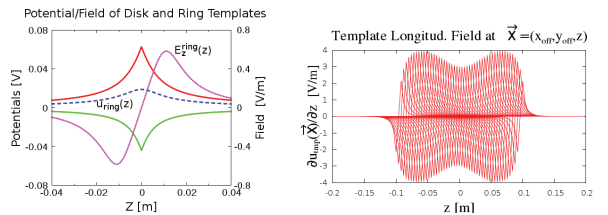


Figure 4: Potentials and a field of disks/ring in free space (left). Template potentials of a beam from right part of Fig. 3 (right).

We benchmarked the results for a 3D $1\text{cm} \times 1\text{cm} \times 10\text{cm}$ ellipsoid, carrying a uniformly distributed space charge of $Q=10^{-11}$ C, placed into a conducting pipe of 4 cm in diameter. The results obtained for disk and for ring templates agreed very well. Figs. 5 shows the same potential and fields as in [11, p.407] at $x_{off}=y_{off}=0$, obtained by SOR 3D, for distributions from Figs. 3. For longer bunches with semiaxes $1\text{cm} \times 1\text{cm} \times 50\text{cm}$, the field flattens in the middle and "ear-fields" appear at the edges.

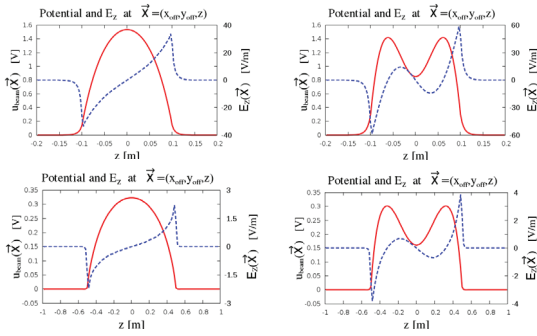


Figure 5: Potentials and fields of 3D ellipsoids with 1cm×1cm×10cm (top), and 1cm×1cm×50cm (bottom).

Fig. 5 suggests that non-linear behavior of longitudinal field becomes very strong due to image forces (in free space, a uniformly charged 3D ellipsoid has linear fields).

A Gaussian 3D beam of ellipsoidal shape in free space has an analytical form of $E_{x,y,z}$ fields (the so-called “frozen” SC model). The presence of a boundary changes them dramatically, limiting their applicability in tracking codes. We refer especially to the longitudinal field E_z , which is most affected by image forces.

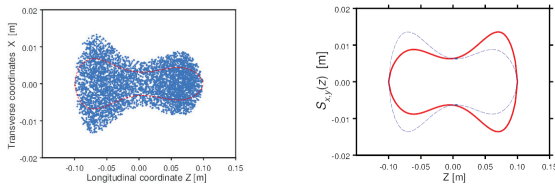


Figure 6: Transverse rms profiles $\langle x^2 \rangle^{1/2}(z)$, $\langle y^2 \rangle^{1/2}(z)$ (left) and shape functions $S_{x,y}(z)$, defining the template shell (right).

The number of templates for accurate space charge calculations is a free parameter. For a beam depicted in Figs. 3, one needs 15-20 templates. “Thick” slices may also be helpful to deal with very long bunches.

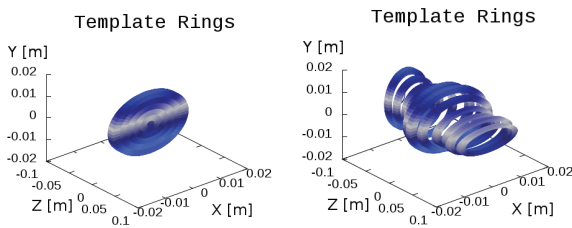


Figure 7: Disk templates (left), built from rings. Ring templates for the outer layer of beam bunch (right).

For a real 3D bunch consisting of macro-particles, Figs. 6 demonstrate the procedure to find shape functions $S_{x,y}(z)$, determining the shell containing all templates, and Fig. 7 illustrates how ring templates reproduce the beam.

Halo and Hollow Beams

For high-brightness accelerators (HL-LHC, ESS), beam loss control is critical, and generally must obey “the 1W/m rule” [12]. While losses may be less than 0.1%, the halo (from which most losses come) may contain a much

larger fraction of a beam, and fields from halo particles can’t be neglected. Numerical noise from halo particles in a regular grid-based PIC may well be unacceptable.

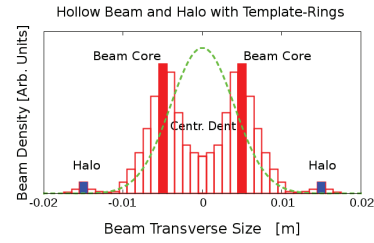


Figure 8: A transversal cross-section of an arbitrary “made-up” hollow beam with a halo, represented by a library of ring templates. An ideal Gaussian beam distribution is a dashed line.

Ring templates are quite appropriate for halo as well as hollow beam field calculations, as shown in Fig. 8. Having disk templates, a special distribution like that would be difficult to reproduce.

DISCUSSION

The goal of this paper is to evaluate accuracies of SC tracking codes for rings, to develop a strategy to suppress artificial numerical effects, and ultimately, to improve code performance. The errors in SC fields will always persist due to granularity of space charge distribution, and inaccuracies of grid density calculations will dominate other errors: a grid Poisson solver and field interpolation and of course those of higher order tracking engines.

A decrease of grid dimensions (larger meshes) damps density fluctuations. The same is valid for larger CIC clouds. However, these fluctuations may be physical, and such a brute force remedy simply eliminates them. A beam halo requires special treatment.

The split operator paradigm is valid for very long bunches (a coasting beam approximation, as in PSR, SNS). For shorter bunches, a more accurate approach is required, based on templates and hybrid technique [5,8].

ACKNOWLEDGEMENTS

The authors are grateful to L. Michelotti, N. Mokhov (FNAL) and A. Friedman (LLNL) for useful discussions.

REFERENCES

- [1] R.W. Hockney, J.W. Eastwood: “Computer Simulation Using Particles”, CRC Press (1988).
- [2] SC13, CERN, Geneva (2013), F.Schmidt et al.
- [3] F.Filbet et al., ICCSA 2002: 305-314.
- [4] L.G.Vorobiev and R.C.York, ibid. 315-324.
- [5] L.G.Vorobiev and R.C.York. Phys. Rev. ST Accel. Beams 3, 114201 (2000), EPAC 2002, p. 1679-1681 (2002).
- [6] Leo Michelotti, et al. PAC 2005, pp. 988-990 (2005).
- [7] L.G.Vorobiev and K.Hirata, KEK-Report 95-12 (1995).
- [8] L.G.Vorobiev, Fermilab Beamdocs, docid=4340 (2013).
- [9] L.G.Vorobiev and R.C.York, PAC 2003, p. 3533 (2003).
- [10] L.G.Vorobiev, Fermilab-Pub-08-236-APC (2008).
- [11] M.Reiser, “Theory and Design of Charged Particle Beams”, John Wiley & Sons, New York (1994).
- [12] N.V.Mokhov et al.: Fermilab-Conf-12-634-APC (2009).